

Effect of suppression of local distortion on magnetic, electrical and thermal transport properties of Cr substituted bi-layer manganite $\text{LaSr}_2\text{Mn}_2\text{O}_7$

M.Matsukawa,* M.Chiba, and E.Kikuchi

Department of Materials Science and Technology, Iwate University, Morioka 020-8551, Japan

R.Suryanarayanan and M.Apostu

*Laboratoire de Physico-Chimie de L'Etat Solide, CNRS,
UMR8648 Universite Paris-Sud, 91405 Orsay, France*

S.Nimori

National Institute for Materials Science, Tsukuba 305-0047, Japan

K. Sugimoto

X-Ray Research Laboratory, Rigaku Corporation, Tokyo 196-8666, Japan

(Dated: November 6, 2018)

We have investigated magnetic, electrical and thermal transport properties (Seebeck effect and thermal conductivity) of $\text{LaSr}_2\text{Mn}_{2-y}\text{Cr}_y\text{O}_7$ polycrystalline samples ($y=0.1, 0.2, 0.4$ and 0.6). The Cr^{3+} substitution for Mn^{3+} sites causes a removal of $d_{x^2-y^2}$ orbital of e_g -electron resulting in a volume shrinkage of lattice. Magnetic measurements reveal the appearance of a glassy behavior for Cr-doped samples, accompanied by both a collapse of the A-type antiferromagnetic structure and the growth of ferromagnetic clusters. Cr-doping effect on electrical transport strongly enhances an insulating behavior over a wide range of temperature, while it suppresses a local minimum of thermoelectric power at lower temperatures. For all polycrystalline samples with Cr-substitution, the variable-range-hopping (VRH) conduction model gives a reasonable fit to both resistivities and Seebeck coefficients. The phonon thermal conduction gradually rises with increasing Cr content, which is in contrast to a typical impurity effect on thermal conductivity. We attribute this to a suppression of local lattice distortion through the introduction of Jahn-Teller inactive ions of Cr^{3+} .

PACS numbers: 75.47.Lx, 75.50.Lk

I. INTRODUCTION

The discovery of colossal magnetoresistance (CMR) effect in doped manganites with perovskite structure has stimulated considerable interest for the understanding of their physical properties¹. Though the insulator to metal (IM) transition and its associated CMR are well explained on the basis of the double exchange (DE) model, it is pointed out that the dynamic Jahn-Teller (JT) effect due to the strong electron-phonon interaction, plays a significant role in the appearance of CMR as well as the DE interaction^{2,3}. Furthermore, Dagotto et al propose a phase separation model where the ferromagnetic (FM) metallic and antiferromagnetic (AFM) insulating clusters coexist and their model strongly supports recent experimental studies on the physics of manganites^{4,5}.

In bilayer manganites $\text{La}_{2-2x}\text{Sr}_{1+2x}\text{Mn}_2\text{O}_7$, in which a MnO_2 bilayer is alternatively stacked with a (La,Sr)₂O₂ blocking layer along the c -axis, the physical properties strongly depend on hole doping level, x ⁶. In particular, neutron diffraction study on half doped $\text{LaSr}_2\text{Mn}_2\text{O}_7$ ($x=0.5$) has revealed the coexistence of the A-type antiferromagnetic (AFM) phase and CE-type antiferromagnetic charge-ordered/orbital-ordered (CO/OO) phase⁷. It is well known that the CE-type CO/OO state in cubic manganites is unstable against Cr-substitution for Mn-site and lightly Cr doping up to

a few percents yields a drastic collapse of the CO/OO phase, resulting in a FM metallic phase even in the absence of any applied magnetic field^{8,9}. While several reports on the effect of Cr substitution on the physical properties of the cubic manganites have appeared, very few reports have appeared on such studies in the case of bilayer manganites^{10,11}. Here, we give some comments on pressure effect on a two-dimensional network of MnO_6 octahedra in bilayer manganites $\text{La}_{1.2}\text{Sr}_{1.8}\text{Mn}_2\text{O}_7$. Argyriou et al¹², reported that the Mn-O(3)-Mn bond angle is almost unchanged by application of pressure, indicating no tilting of the MnO_6 octahedra in the ab plane. Thus, it is possible to examine the internal and external pressure effect in bilayered manganites, varying the bond length of the MnO_6 octahedra but keeping the bond angle almost 180°. In this paper, we report magnetic, electrical and thermal transport properties of single-phase $\text{LaSr}_2\text{Mn}_{2-y}\text{Cr}_y\text{O}_7$ polycrystalline samples ($y=0.1, 0.2, 0.4$ and 0.6). The Cr-substitution for Mn sites causes a monotonic shrink of $a(b)$ -axis in contrast with a gradual elongation of c -axis, accompanied by $d_{x^2-y^2}$ orbital deficiencies of e_g -electron as listed in Table I. The $3d$ electronic state of Cr^{3+} ion is taken as $t_{2g}^3 e_g^0$ (spin quantum number $S=3/2$), resulting in undistorted CrO_6 octahedron sites free from local Jahn-Teller effect. This finding is quite reasonable with a volume shrinkage observed due to Cr-doping because a removal of $d_{x^2-y^2}$ orbital

from Mn^{3+} sites easily causes a suppression of local lattice distortion as discussed later. In the parent material $\text{LaSr}_2\text{Mn}_2\text{O}_7$, a majority phase of the A-type AFM state coexists with a minority phase of CE-type AFM charge-ordered/orbital-ordered state⁷. We focus our attention on Cr-doping effect on the A-type AFM majority phase because it is expected that the CO/OO minority phase is strongly suppressed by Cr-doping.

II. EXPERIMENT

Polycrystalline samples of $\text{LaSr}_2\text{Mn}_{2-y}\text{Cr}_y\text{O}_7$ ($y=0.1, 0.2, 0.4$ and 0.6) were synthesized by solid-state reaction of La_2O_3 , SrCO_3 , MnO_2 and Cr_2O_3 powders with high purity. The oxygen concentration of typical samples with $y=0.2$ and 0.6 was determined using the infrared absorption method because the existence of the Cr ions may affect the valence estimation of Mn ion made by the chemical analysis. The composition of cations was examined by inductively coupled plasma analysis. For the $y=0.2$ and 0.6 samples, we got $\text{La}_{1.02}\text{Sr}_{2.01}\text{Mn}_{1.83}\text{Cr}_{0.19}\text{O}_{6.99}$ at $y = 0.2$ and $\text{La}_{1.01}\text{Sr}_{1.95}\text{Mn}_{1.41}\text{Cr}_{0.59}\text{O}_{7.05}$ at $y = 0.6$. Thus, we conclude that our samples prepared by the solid state reaction technique are close to nominal compositions. Let us consider the difference in oxygen concentration (hole concentration). The values of $7-\delta=6.99$ at $y=0.2$ and $7-\delta=7.05$ at $y=0.6$ give hole contents of $x=0.5$ and $x=0.55$, respectively. Recent neutron powder diffraction studies on $\text{La}_{2-2x}\text{Sr}_{1+2x}\text{Mn}_2\text{O}_7$ revealed the magnetic and crystallographic phase diagram in the region $x > 0.5$ ¹³. In particular, when $0.42 < x < 0.66$, appears the A-type AFI state with antiferromagnetic coupling along the c -axis between FM single layers within one bilayer. We believe that the excess oxygen content ($x=0.55$) gives little effect on the magnetic property because the AFM magnetic transition temperature is stable over the range of hole concentration up to $x = 0.6$.

The x-ray powder diffraction patterns were recorded for all samples on a RIGAKU diffractometer with $\text{CuK}\alpha$ radiation as depicted in Fig.1. The x-ray data are indexed in terms of $(\text{La,Sr})_3\text{Mn}_2\text{O}_7$ 327 phase except for a small amount of impurity phase, indicating a single phase of bilayered structure. The lattice parameters calculated using the least squared fits are listed in Table I as a function of Cr-content.

Magnetic measurements as a function of temperature were carried out using a SQUID magnetometer in both zero-field-cooled (ZFC) and field-cooled (FC) scans. The magnetic relaxation was measured as follows; First, the sample was cooled down to the respective temperatures in a zero field and then the applied field was held for 5 minutes. Finally, just after the field was switched off, remanent magnetization data were recorded as a function of time. Electrical resistivity was measured by a conventional four-probe technique. Magnetoresistance measurements were performed at National Institute for Materials Science. Here, an electric current supplied was parallel

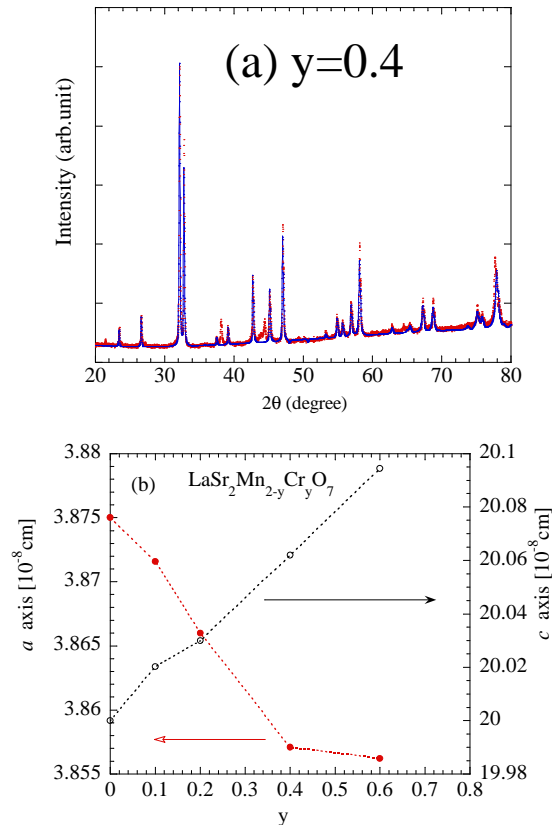


Fig. 1: (Color online) (a) The x-ray powder diffraction pattern on the $y=0.4$ sample. Dots and a solid line are the observed and calculated intensities. The x-ray data are indexed in terms of $(\text{La,Sr})_3\text{Mn}_2\text{O}_7$ 327 phase except for a small amount of impurity phase. (b) The lattice parameters calculated using the least squared fits as a function of Cr-content as listed in Table I.

TABLE I: The lattice parameters, a and c , A-type AFM transition temperature T_N , spin-glass like transition temperature T_{SG} . The T_N is determined from a local maximum at higher T in ZFC data while T_{SG} is defined from the prominent peak located at low- T . The lattice parameters of singlecrystalline $\text{LaSr}_2\text{Mn}_2\text{O}_7$ are taken from ref.¹⁵.

Sample	a	c	T_N	T_{SG}
y	(\AA)	(\AA)	(K)	(K)
0	3.8790	19.996	210	
0.1	3.8716	20.020	175	
0.2	3.8660	20.030	130	
0.4	3.8571	20.062		38
0.6	3.8562	20.094		34.5

to the direction of the external field. The thermal conductivity was measured using a conventional heat-flow method. The thermoelectric power S ($=dV/dT$) was determined both from a temperature gradient and thermoelectric voltage, dT and dV , which are generated from a thermal current in the longitudinal direction of samples.

III. RESULTS AND DISCUSSION

A. Magnetic property

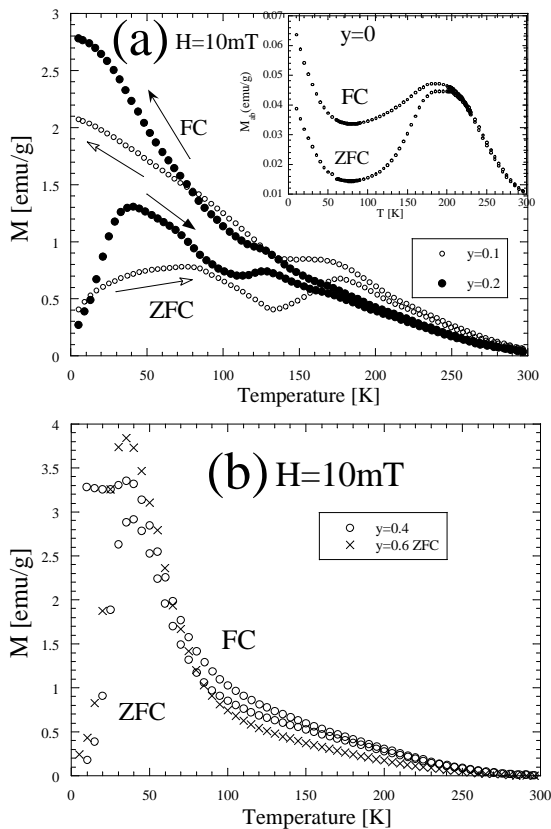


Fig. 2: ZFC and FC temperature dependences of the magnetization in polycrystalline $\text{LaSr}_2\text{Mn}_{2-y}\text{Cr}_y\text{O}_7$ ($y=0.1, 0.2, 0.4$ and 0.6), measured at 10 mT. For comparison, the ab -plane magnetization data of parent crystal $\text{LaSr}_2\text{Mn}_2\text{O}_7$ are presented in the inset of (a).

First, let us show in Fig. 2 the ZFC and FC temperature dependences of the magnetization in polycrystalline $\text{LaSr}_2\text{Mn}_{2-y}\text{Cr}_y\text{O}_7$ ($y=0.1, 0.2, 0.4$ and 0.6), measured at 10 mT. For comparison, the ab -plane magnetization data of parent crystal $\text{LaSr}_2\text{Mn}_2\text{O}_7$ are presented in the inset of Fig. 2¹⁴. Upon cooling the Cr-free sample, a broad maximum in M_{ab} is observed near about 210K, associated with the A-type AFM transition^{15,16}. Cr-doping strongly suppresses Neel temperature T_N , from 210 K at $y=0$, through 175K at $y=0.1$, down to 130K at $y=0.2$ and such a magnetic anomaly finally disappears for the $y=0.4$ and 0.6 samples. The T_N is determined from a local maximum at higher temperatures in ZFC data. In the A-type AFM structure, FM spins lying in ab -plane of respective MnO_2 single layer are antiferromagnetically coupled along the c -axis within a MnO_2 double layer. We expect that a partial substitution of Cr^{3+} for Mn^{3+} sites causes $d_{x^2-y^2}$ orbital deficiencies of

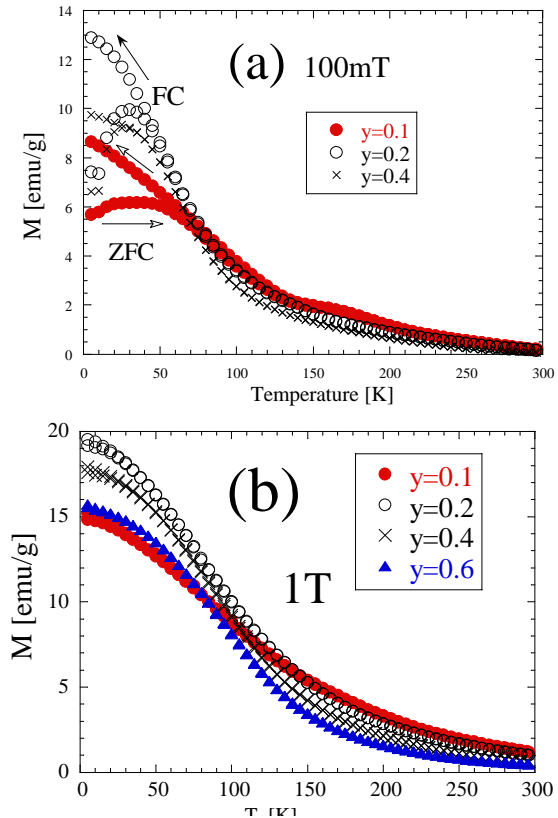


Fig. 3: (Color online) ZFC and FC temperature dependences of the magnetization in polycrystalline $\text{LaSr}_2\text{Mn}_{2-y}\text{Cr}_y\text{O}_7$ ($y=0.1, 0.2$ and 0.4), measured in a field of (a) 100mT and (b) 1 T.

e_g -electron and weakens a AFM coupling working between respective single layers, resulting in an observed drop of T_N . Instead, a low- T peak in ZFC scan rapidly grows with Cr-doping, accompanied by a hysteresis region surrounded between ZFC and FC curves. At further low temperatures, the ZFC magnetization of $y=0.2-0.6$ shows a steep decrease, indicating the freezing of magnetic moments^{17,18}. These findings are reminiscent of magnetic behaviors of a standard spin-glass system due to a magnetic frustration between ferromagnetic and antiferromagnetic interactions¹⁹. A characteristic temperature where the prominent peak in ZFC scan is located at low- T is defined as T_{SG} for the $y=0.4$ and 0.6 samples at 10mT. In addition, the temperature variation of magnetization polycrystalline $\text{LaSr}_2\text{Mn}_{2-y}\text{Cr}_y\text{O}_7$ ($y=0.1, 0.2$ and 0.4) both in 0.1 T and 1T is shown in Fig. 3. At 0.1T, a history effect between ZFC and FC scans remains visible at lower- T . However, at relatively high field of 1T, the irreversibility in magnetization curves is strongly suppressed and a ferromagnetic-like behavior appears at low temperatures. These tendencies depending on the applied fields are never observed in a conventional spin-glass system.

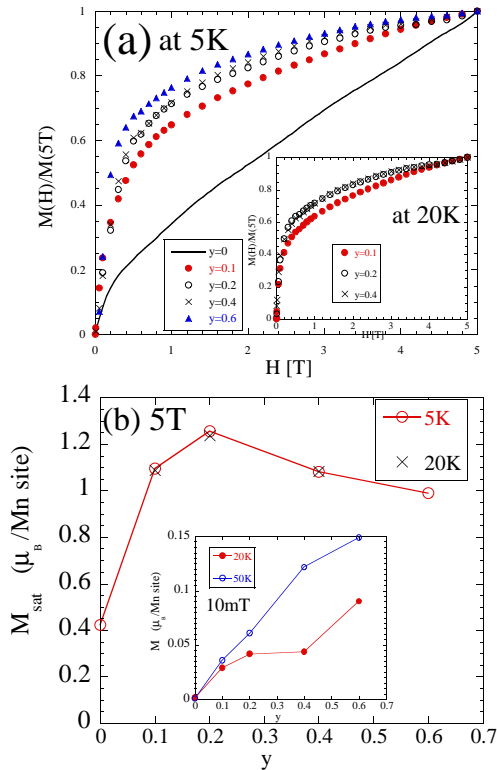


Fig. 4: (Color online) (a) Field dependence of the magnetization at 5K in $\text{LaSr}_2\text{Mn}_{2-y}\text{Cr}_y\text{O}_7$ ($y=0.1,0.2,0.4$ and 0.6). The $M(H)$ data at 20K are also given in the inset of (a). (b) The saturated magnetization at 5T as a function of Cr-content. For comparison, the low-field magnetization is plotted as a function of Cr-content in the inset of (b).

Next, we examine the field dependence of low- T magnetization in $\text{LaSr}_2\text{Mn}_{2-y}\text{Cr}_y\text{O}_7$ ($y=0.1,0.2,0.4$ and 0.6) (Fig. 4 (a)). The ab -plane magnetization of the Cr-free crystal shows a linear dependence on the field, in association with an AFM spin canting induced by the external field¹⁶. On the other hand, in Cr-doped samples, $M-H$ curves rapidly rise at low fields and then tend to saturate up to a maximum field of 5T, indicating the development of ferromagnetic states. Upon increasing Cr-doping, the initial M shows a steeper rise. Let us show in Fig. 4 (b) the saturated magnetization at 5T plotted as a function of Cr-content. We notice that the saturated magnetic moment M_{sat} is almost independent of Cr-impurities in strong contrast to Cr-substitution effect on low-field magnetization in the inset of Fig. 4(b). It is true that Cr-impurity induces ferromagnetic moment from the inset of Fig. 4 (b), but the volume fraction of FM phase at 5T is almost insensitive of Cr content. The value of $M_{sat}(5T)$ is converged within 30 to 35 percents of full ferromagnetic moment. ($M_{full}=3.4 \mu_B$ at $y=0.2$ and $M_{full}=3.2 \mu_B$ at $y=0.6$.) We give

some comments on the apparent disagreement in Cr-substitution effect between low and high field magnetic properties. A partial substitution of Cr^{3+} ion for Mn^{3+} suppresses not only AFM coupling between single MnO_2 layers but also destroys FM double-exchange interaction between Mn^{3+} and Mn^{4+} ions within the MnO_2 layer. It is expected that the addition of Cr^{3+} ions causes a suppression of FM region mediated by DE interaction through removing Mn^{3+} ions. On the other hand, the low field data support the occurrence of the ferromagnetic moment induced by Cr substitution. Following the Kanamori-Goodenough rules, the superexchange(SE) interaction between Cr^{3+} ($t_{2g}^3 e_g^0$) and Mn^{3+} ($t_{2g}^3 e_g^1$) ions is ferromagnetic while the SE interaction between Cr^{3+} and Mn^{4+} ($t_{2g}^3 e_g^0$) becomes antiferromagnetic²⁰. The annihilation of the $\text{Mn}^{3+} - \text{Mn}^{4+}$ FM pairs is compensated by the creation of the $\text{Cr}^{3+} - \text{Mn}^{3+}$ FM pairs accompanied by the $\text{Cr}^{3+} - \text{Mn}^{4+}$ AFM pairs. In other words, the DE driven FM regions are partially replaced by the SE driven FM regions with increasing the Cr ions, keeping the total FM fraction. The FM double-exchange interaction between Mn^{3+} and Cr^{3+} is not possible in our samples because the occurrence of FM moment by Cr-doping accompanies no metallic property as discussed later in the Cr-doping effect on resistivity. At high fields, the phase separation between the field-induced FM phase and AFM second phase is probably realized at the level of clusters on the basis of the competition between FM and AFM interaction. Next, we carried out the magnetic relaxation of the $y=0.4$ sample in order to examine the glassy state below T_{SG} . In Fig.5, we show the remanent magnetization data of the $y=0.4$ sample as a function of time, just after holding an applied field for 5 minutes and then switching it off. At 10mT, the magnetization relaxes faster at lower- T , in contrast with the $M(t)$ data at 100mT. However, at 1T no slow relaxation in M is observed, which is consistent with no history effect in ZFC and FC scans. The slow decay of remanent magnetization curves indicates that a difference in free energy between the present excited and ground states is quite small in comparison with thermal energy and the system remains stable in various excited states^{21,22,23}. Thus, a relatively fast relaxation of remanent M at 10K in 10mT scan leads to a larger difference of energy barrier between the ground and excited states than in the case of 100mT at the same temperature. The metastable state excited by the lower field is probably related to the degree of a magnetic frustration between AFM and FM clusters and/or the spatial distribution of frustrated clusters. Furthermore, the coexistence of frustrated clusters and ferromagnetic clusters plays a crucial role in the magnetic relaxation in 100mT. FM spins and/or FM domain walls are pinned on the lattice defect sites like oxygen vacancy, giving a longer relaxation time.

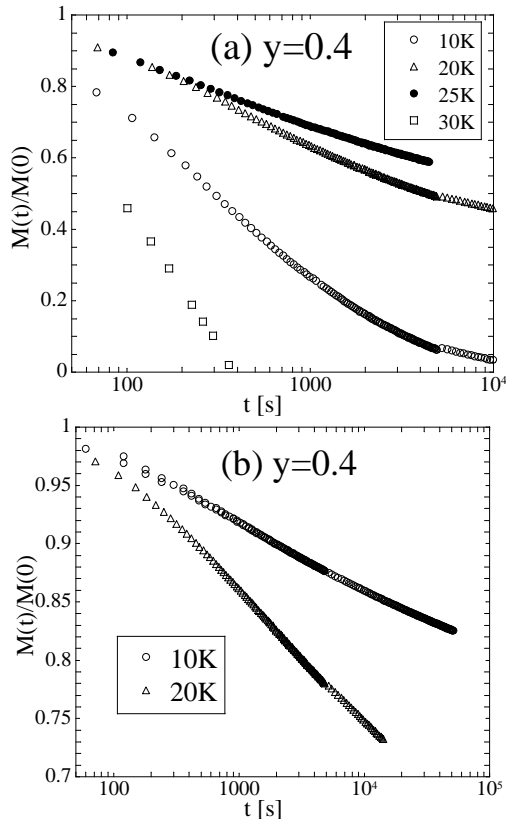


Fig. 5: Remanent magnetization data of the $y=0.4$ sample as a function of time, just after holding an applied field H_a for 5 minutes and then switching it off. (a) $H_a=10\text{mT}$ and (b) $H_a=100\text{ mT}$.

B. Electrical transport property

Figure 6 displays the temperature dependence of the electrical resistivity in polycrystalline $\text{LaSr}_2\text{Mn}_{2-y}\text{Cr}_y\text{O}_7$ ($y=0.1, 0.2, 0.4$ and 0.6). For comparison, the resistivity data of parent crystal $\text{LaSr}_2\text{Mn}_2\text{O}_7$ are also presented in Fig.6. The value of ρ at lower T exhibits a rapid increase by about four orders of magnitude, from $\sim 10^2\ \Omega\text{cm}$ at $y=0.1$ up to $10^6\ \Omega\text{cm}$ at $y=0.4$. Cr-doping strongly enhances an insulating behavior over a wide range of temperature because conduction paths are partially destroyed by $d_{x^2-y^2}$ orbital deficiencies of e_g -electron. Our data exclude in this system a possibility of the global double-exchange interaction between Mn^{3+} and Cr^{3+} ions, giving a metallic property²⁴. In particular, for the $y=0-0.2$ sample, the rapid rise in $\rho(T)$ below 50K is close to carrier localization effect due to a suppression of carrier hopping between single layers because at lower- T orbital fluctuation of $d_{x^2-y^2}$ is gradually suppressed and motion of carriers are confined within respective single layer¹⁶.

We try to analyze the $\rho(T)$ data of Cr-doped samples using the small-polaron hopping model and Mott's

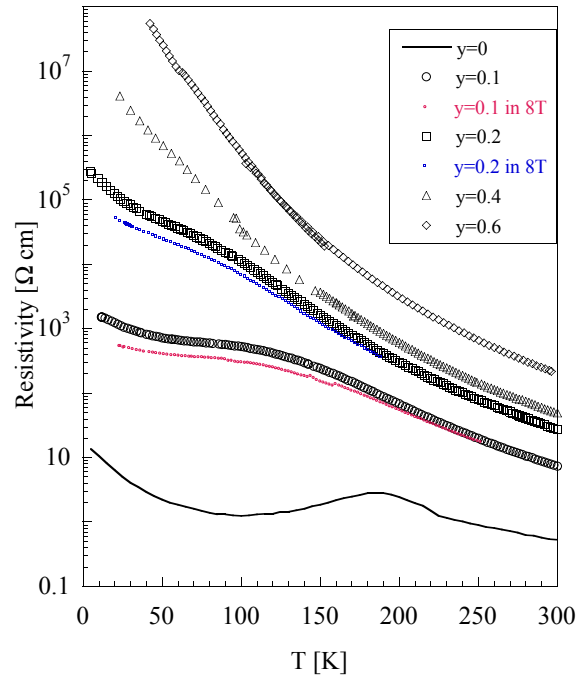


Fig. 6: (Color online) Temperature dependence of the electrical resistivity in polycrystalline $\text{LaSr}_2\text{Mn}_{2-y}\text{Cr}_y\text{O}_7$ ($y=0.1, 0.2, 0.4$ and 0.6). For comparison, the resistivity data of single crystalline $\text{LaSr}_2\text{Mn}_2\text{O}_7$ are also presented.

TABLE II: The fitting parameters, ρ_0 and T_0 for polycrystalline samples of $\text{LaSr}_2\text{Mn}_{2-y}\text{Cr}_y\text{O}_7$ ($y=0.1, 0.2, 0.4$ and 0.6)

Sample	VRH regime	2D VRH		3D VRH	
		ρ_0 (Ωcm)	T_0 (K)	ρ_0 (Ωcm)	T_0 (K)
0.1	$T > 187$	2.1×10^{-6}	1.0×10^6	8.7×10^{-9}	5.4×10^7
0.2	$T > 161$	3.0×10^{-6}	1.2×10^6	8.1×10^{-9}	7.0×10^7
0.4	$T > 155$	2.0×10^{-6}	1.5×10^6	3.7×10^{-9}	8.9×10^7
0.6	$T > 113$	2.6×10^{-6}	1.8×10^6	2.7×10^{-9}	1.2×10^8

variable-range-hopping (VRH) model²⁵, to examine the conduction mechanism of bilayered manganites²⁶. According to Mott's VRH model, the temperature dependence of resistivities is represented by $\rho(T)=\rho_0\exp[(T_0/T)^p]$, where ρ_0 is a constant and $p = 1/(d + 1)$ with d being the dimensionality of the system. Mott's activation energy T_0 is proportional to $1/[N(E)\xi^d]$, where $N(E)$ is the density of states at the Fermi level and ξ is the localization length. On the other hand, the adiabatic small-polaron model is described by $\rho(T)=\rho_0T\exp(E_p/kT)$, where ρ_0 is a constant and E_p represents the activation energy of small-polaron. For all

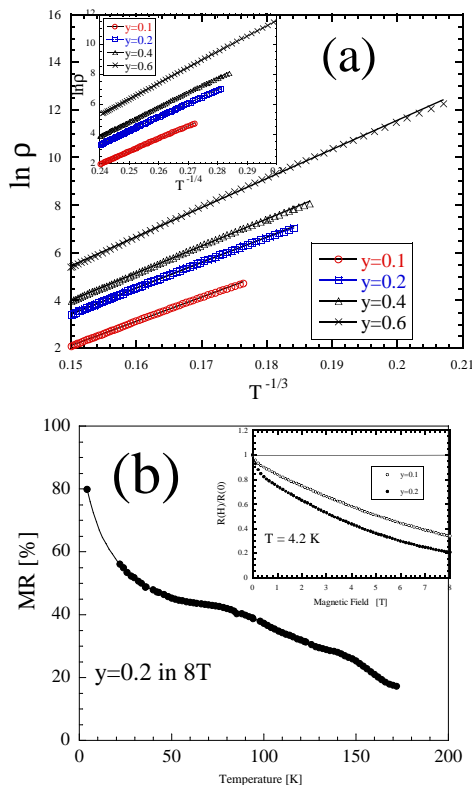


Fig. 7: (Color online) (a) a semilog plot of ρ versus T^{-p} with $p = 1/3$ for $\text{LaSr}_2\text{Mn}_{2-y}\text{Cr}_y\text{O}_7$ ($y=0.1, 0.2, 0.4$ and 0.6). The solid lines correspond to fits by Mott's VRH model. The inset also presents a semilog plot of ρ versus T^{-p} with $p = 1/4$ for 3D VRH. With increasing Cr-doping level, the VRH regime is extended as listed in Table II. (b) Magnetoresistance effect of the $y=0.2$ sample as a function of temperature at 8T. In the inset, the MR of $y=0.1$ and 0.2 samples at 4.2K is plotted as a function of field up to 8T.

samples with Cr-substitution, it is found that the VRH model gives a more reasonable fit to the experimental data over a wide range of temperatures, in comparison with the small-polaron model. In Fig.7(a), we present our results as a semilog plot of ρ versus T^{-p} with $p = 1/3$ for 2D VRH, while the inset of Fig.7(a) shows a semilog plot of ρ versus T^{-p} with $p = 1/4$ for 3D VRH. Although it is hard to distinguish a $T^{-1/3}$ or $T^{-1/4}$ dependence of $\ln\rho$, we obtain a much better fit to Mott's VRH than to a VRH model with $p = 1/2$ in the presence of Coulomb gap^{26,27}. The fitting parameters, ρ_0 and T_0 , for polycrystalline samples of $\text{LaSr}_2\text{Mn}_{2-y}\text{Cr}_y\text{O}_7$ ($y=0.1, 0.2, 0.4$ and 0.6) are listed in Table II. With increasing Cr-content, the value of T_0 shows a monotonous increase for both 2D and 3D cases, indicating the decrease of the localization length ξ . The localization effect enhanced due to Cr-substitution is probably associated with orbital disorders in Mn-O-Mn networks introduced by the removal of e_g -electron^{28,29}.

We give some comments on the doping effect of other trivalent metallic ions (Co^{3+} and Al^{3+}) on the Mn sites of $\text{La}_1\text{Sr}_2\text{Mn}_2\text{O}_7$ ^{28,29}. The $3d$ electronic configuration of Co^{3+} ion follows as; $t_{2g}^6e_g^0$ ($S=0$, low-spin state), $t_{2g}^5e_g^1$ ($S=1$, intermediate -spin state) and $t_{2g}^4e_g^2$ ($S=2$, high-spin state). The Al^{3+} ion is a non magnetic ion without d -electrons. With increasing Co^{3+} (or Al^{3+}) doping level, the A-type AFM temperature shifts to low temperatures and the magnitude of magnetization decreases over a wide range of temperatures. The decrease of M implies a reduction of the net magnetic moments, which is consistent with low-spin state ($S=0$) of Co^{3+} or non magnetic ion of Al^{3+} . The latter tendency is in strong contrast with the magnetic effect of Cr^{3+} ($t_{2g}^3e_g^0, S=3/2$) doping on $\text{La}_1\text{Sr}_2\text{Mn}_2\text{O}_7$ although a suppression of A-type-AFM temperature is commonly observed for Cr, Co and Al doping. On the other hands, the doping effects on electrical transport for Cr, Co and Al ions exhibit such common features as the enhanced insulating state due to orbital deficiencies following the VRH model. In particular, the Al substitution without d -electrons for Mn site products a more rapid increase in resistivities.

Magnetoresistance(MR) effect of the $y=0.2$ sample as a function of temperature is depicted in Fig.7 (b), where the negative MR is defined as $-100 \cdot [\rho(8\text{T}) - \rho(0\text{T})] / \rho(0\text{T})$. The value of giant MR increases from 25 % at 150K up to 80 % at 4.2K with decreasing T . The existence of the field-induced FM clusters is probably related to the enhanced MR at low temperatures as we see from MT data in Fig.3(b). In the inset of Fig. 7 (b), the MR of $y=0.1$ and 0.2 samples is plotted as a function of field up to 8T. Cr-doping also increases a low- T MR from 45 % at $y=0.2$ up to 80 % at $y=0.6$ under a field of 8T at 40K. The Cr-doping induced orbital disorders assist charge transfer along the c -axis across respective single layer of MnO_2 , giving the enhanced MR effect.

C. Thermal transport properties (Seebeck effect and thermal conductivity)

Next, the temperature variation of Seebeck coefficient S for the $y=0.1-0.6$ samples is displayed in Fig.8(a). For comparison, the $S(T)$ data of single crystalline $\text{LaSr}_2\text{Mn}_2\text{O}_7$ are cited¹⁴. For $y=0-0.2$, with decreasing T , the value of $S(T)$ shows a local maximum near the A-type AFM transition temperature T_N and then a shallow minimum at lower T is observed³⁰. At lower T , Cr-doping gradually suppresses a local minimum of $S(T)$ from a negative value at $y=0$ down to a small one at $y=0.2$ and finally at $y=0.4$ the local minimum in $S(T)$ disappears, giving a monotonous decrease over the observed temperature range. Now, let us try to analyze the $S(T)$ data of Cr-doped samples using the extended Mott's VRH model to Seebeck coefficients^{25,31}. For the 2D VRH case, the corresponding form is described by $S(T) \propto T^p$ with $p = 1/3$ ($p = 1/2$ for the 3D VRH case). In Fig.8(b), we present our results as a linear plot

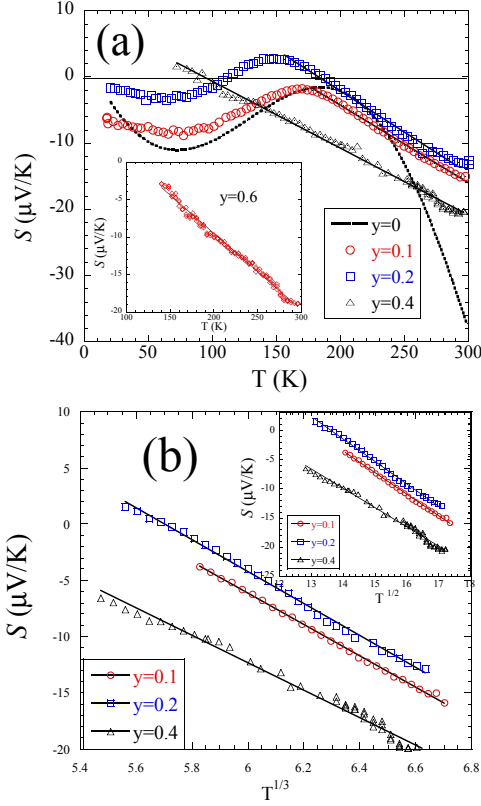


Fig. 8: (Color online) (a) Temperature variation of Seebeck coefficient S for $\text{LaSr}_2\text{Mn}_{2-y}\text{Cr}_y\text{O}_7$ ($y=0, 0.1, 0.2$ and 0.4). The solid lines correspond to T linear fits. The inset represents the S data of the $y=0.6$ sample with a linear fit. (b) Seebeck coefficient $S(T)$ versus $T^{1/2}$ for $\text{LaSr}_2\text{Mn}_{2-y}\text{Cr}_y\text{O}_7$ ($y=0.1, 0.2$ and 0.4). The solid lines correspond to fits by the 2D VRH model. The inset presents $S(T)$ versus $T^{1/3}$ for the 3D VRH model. In the case of $y=0.2$, we have typical fitting parameters $A=77 \mu\text{V/K}$ and $B=14 \mu\text{V/K}^{3/2}$ for 2D VRH ($A=52 \mu\text{V/K}$ and $B=3.8 \mu\text{V/K}^{4/3}$ for 3D VRH), where $S(T) = A - BT^p$. The $S(T)$ of the $y=0.2$ follows the VRH law for $169 \text{ K} \leq T \leq 300 \text{ K}$

of $S(T)$ versus $T^{1/2}$ for 2D VRH (in the inset, $S(T)$ versus $T^{1/3}$ for 3D VRH). In a similar way, we obtain a much better fit of $S(T)$ data to the VRH law than to the thermally activated T dependence. Here, the Seebeck coefficient for a thermally activated case is expressed as $S(T) = k/e(E_S/kT) + S_\infty$, where E_S is a thermal activation energy and S_∞ denotes Seebeck coefficient in the high temperature limit. In addition, the obvious differences among the T , $T^{1/2}$ and $T^{1/3}$ dependences we do not notice within our fitting procedures. In the random hopping system, the T -linear dependence of $S(T)$ is theoretically presented by Culter and Mott³². The T -linear dependence of $S(T)$ in the insulating state is probably related to a random distribution of localized electronic states around Fermi level as reported in Seebeck coefficient of $\text{Li}_{1+x}\text{Ti}_{2-x}\text{O}_4$ oxides ref.³³.

In a doped bilayer manganite with hole content $x=0.4$, the high temperature behavior of $S(T)$ is well explained on the basis of a model of Zener polarons, where a Zener polaron formed in the high- T region occupy two manganese sites³⁴. It is true that this model qualitatively reproduces a negative sign in high- T behavior of single crystalline $\text{La}_1\text{Sr}_2\text{Mn}_2\text{O}_7$. However, for all polycrystalline samples with Cr-substitution it seems that the VRH conduction gives a reasonable fit to both resistivities and Seebeck coefficients.

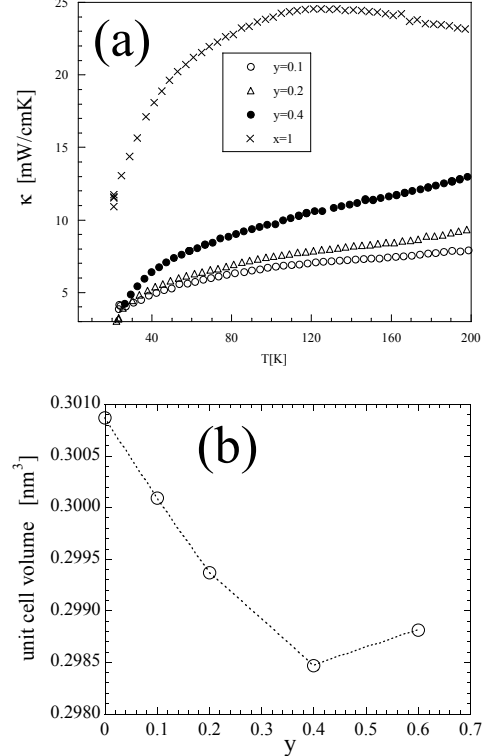


Fig. 9: (a) Temperature dependence of thermal conductivity for $\text{LaSr}_2\text{Mn}_{2-y}\text{Cr}_y\text{O}_7$ ($y=0.1, 0.2$, and 0.4). For comparison, the κ data of polycrystalline $\text{Sr}_3\text{Mn}_2\text{O}_7$ ($x=1$) is presented. (b) the unit-cell volume of $\text{LaSr}_2\text{Mn}_{2-y}\text{Cr}_y\text{O}_7$ as a function of Cr-content.

Finally, let us show in Fig.9 the thermal conductivity of Cr-doped $\text{LaSr}_2\text{Mn}_{2-y}\text{Cr}_y\text{O}_7$ ($y=0.1, 0.2$, and 0.4) as a function of temperature. For comparison, the κ data of polycrystalline $\text{Sr}_3\text{Mn}_2\text{O}_7$ ($x=1$) is presented³⁵. First of all, thermal carries are phonons since the electron component is estimated to be negligible from the resistivity data using the Wiedemann-Franz law. The phonon thermal conduction gradually increases with Cr-doping, which seems to be an unusual behavior because the introduction of Cr-impurity ions would disturb phonon conduction. However, this anomalous finding is reasonably resolved through clarifying a close relationship between phonon conduction and local lattice distortion of MnO_6

due to Jahn-Teller effect. In our previous work on thermal conductivity in bilayered manganite single crystals, it has been made clear that the phonon conduction in the insulating state is scattered by local lattice distortions of $\text{Mn}^{3+} \text{O}_6$ but the metallic state realized by lowering of T or by the applied field yields a upturn in κ below T_C or giant magnetothermal effect³⁵. This enhanced phonon conduction arises from a suppression of $\text{Mn}^{3+} \text{O}_6$ local distortions due to a screening effect of itinerant carriers. Cr-substitution for Mn^{3+} sites removes $d_{x^2-y^2}$ orbitals of e_g -electron, resulting in a $\text{Cr}^{3+} \text{O}_6$ octahedron without local JT effect. In other words, Cr-doping effect on lattices causes a suppression of local lattice distortion through the introduction of JT inactive ions, giving an increase in phonon conduction. Surely, the $\kappa(T)$ of polycrystalline $\text{Sr}_3\text{Mn}_2\text{O}_7(x=1)$ shows a typical phonon conduction, whose behavior is free from JT distortion of $\text{Mn}^{3+} \text{O}_6$. In addition, the Cr-doping dependence of a - and c - axis lattice parameters in Table I reveals the volume shrinkage of the unit cell with increasing Cr-content as shown in Fig. 8 (b). We note that the lattice constant of $y=0.6$ is influenced by a small amount of the impurity phase. This volume effect is associated with a number of deficiencies of $d_{x^2-y^2}$ orbitals of e_g -electron, which is quite consistent with the preceding discussion on the close relationship between the lattice distortion and phonon conduction.

IV. SUMMARY

We have carried out magnetic, electrical, Seebeck effect and thermal conductivity measurements of $\text{LaSr}_2\text{Mn}_{2-y}\text{Cr}_y\text{O}_7$ polycrystalline samples ($y=0.1, 0.2, 0.4$ and 0.6). The Cr^{3+} substitution for Mn^{3+} sites produces a monotonic shrink of $a(b)$ -axis in contrast with a gradual elongation of c -axis in association with a removal

of $d_{x^2-y^2}$ orbital of e_g -electron. For Cr-doped samples, a glassy behavior appears accompanied by both a collapse of the A-type antiferromagnetic property and the development of ferromagnetic clusters. At high fields, the irreversibility in magnetization curves disappears and the saturated magnetic moment induced by the applied field reaches 30 to 35 percents of full ferromagnetic moment at 5T for all Cr doped samples. This finding strongly suggests the presence of a phase separation between FM and second phases at the level of clusters, which originates from the frustration between FM and AFM interactions. The electrical transport for Cr-doped samples strongly enhances an insulating property over the wide range of temperature because conduction paths are partially destroyed by $d_{x^2-y^2}$ orbital deficiencies of e_g -electron. At lower T , Cr-doping gradually suppresses a local minimum of $S(T)$ from a relatively large value at $y=0$ down to a positively small one at $y=0.4$ in striking contrast to the more enhanced low- T resistivity data. For all polycrystalline samples with Cr-substitution it seems that the VRH conduction gives a reasonable fit to both resistivities and Seebeck coefficients. The phonon thermal conduction gradually increases with increasing Cr content, which is contrast to a typical impurity effect on thermal conductivity. We propose that the increase in the phonon thermal conduction results from a suppression of local lattice distortion through the introduction of Jahn-Teller inactive ion of Cr^{3+} .

Acknowledgments

This work was partially supported by a Grand-in-Aid for Scientific Research from the Ministry of Education, Science and Culture, Japan. The authors thank Mr. H.Noto and Dr. S. Ueda for their technical supports.

* Electronic address: matsukawa@iwate-u.ac.jp

¹ Colossal Magnetoresistive Oxides, edited by Y.Tokura (Gordon and Breach, New York, 2000).

² C.Zener, Phys.Rev.82,403(1951); P.G.deGennes, *ibid.*118,141 (1960).

³ A.J.Millis, P.B.Littlewood, and B.I.Shraiman, Phys.Rev.Lett.74,5144(1995); A.J.Millis, B.I.Shraiman, and R.Mueller, *ibid.*77,175 (1996).

⁴ For a recent review, see E.Dagotto, T.Hotta, and A.Moreo, Phys.Rep.344,1 (2001).

⁵ E.Dagotto, Nonoscale Phase Separation and Colossal Magnetoresistance (Springer-Verlag, Berlin, 2003).

⁶ K.Hirota, Y.Moritomo, H.Fujioka, M.Kubota, H.Yoshizawa, and Y.Endoh, J.Phys.Soc.Jpn.67,3380(1998).

⁷ M.Kubota, H.Yoshizawa, Y.Moritomo, H.Fujioka, K.Hirota and Y.Endoh, J.Phys.Soc.Jpn.68,2202(1999).

⁸ B.Raveau, A.Maignan, and C.Martin, J.Solid State Chem.130,162 (1997).

⁹ T.Kimura, Y.Tomioka, R.Kumai, Y.Okimoto and Y.Tokura, Phys.Rev.Lett.83,3940(1999).

¹⁰ R.Gundakaram, J.L.Lin, F.Y.Lee, M.F.Tai, C.H.Shen, R.S.Liu and C.H.Huang, J.Phys. Condens. Matter 11,5187(1999).

¹¹ K.B.Chashka, B.Fisher, J.Genossar, A.Keren, L.Patlagan and G.M.Reisner, E.Shimshoni and J.F.Mitchell, Phys.Rev.B65,5144(2002).

¹² D.N.Argyriou, J.F.Mitchell, J.B.Goodenough, O.Chmaissem, S.Short, and J.D.Jorgensen, Phys.Rev.Lett.78,1568(1997).

¹³ C.D.Ling, J.E.Millnurn, J.F.Mitchell, D.N.Argyriou, J.Linton, and H.N.Bordallo, Phys.Rev.B62,15096(2000).

¹⁴ M.Matsukawa, E.Kikuchi, M.Yoshizawa, M.Apostu, R.Suryanarayanan, A.Revcolevschi, and N.Kobayashi, Physica B329-333,900(2003).

¹⁵ R.Suryanarayanan, G.Dhalenne, A.Revcolevschi, W.Prellier, J.P.Renard, C.Dupas, W.Caliebe, and T.Chatterji, Solid State Comm. 113, 267(2000).

- ¹⁶ T.Kimura,R.Kumai,Y.Tokura,J.Q.Li, and Y.Matsui, Phys.Rev.B58, 11081(1998).
- ¹⁷ J.Dho,W.S.Kim, and N.H.Hur, Phys.Rev.B65,024404(2001).
- ¹⁸ M.Apostu, R.Suryanarayanan, A.Revcolevschi, H.Ogasawara, M.Matsukawa, M.Yoshizawa, and N.Kobayashi,Phys.Rev.B64,012407(2001).
- ¹⁹ J.A.Mydosh,SpinGlasses; an Experimental Introduction (Tayler & Francis,London,1993).
- ²⁰ J.B.Goodenough, Magnetism and the Chemical Bond (Interscience,New York,1963).
- ²¹ R. Mathieuet al., Phys.Rev.B63,174405-1(2001).
- ²² I.G.Deac et al., Phys.Rev.B65,174426-1(2002).
- ²³ I.Gordon,P.Wagner,V.V.Moshchalkov,Y.Bruynseraede, M.Apostu, R.Suryanarayanan,and A.Revcolevschi, Phys.Rev.B64,092408(2001).
- ²⁴ Y.Sun, W.Tong, X.Xu,and Y. Zhang, Phys.Rev.B63,174438-1(2001).
- ²⁵ N.F.Mott and E.A.Davies,Electronic Processes in Noncrystalline Solids, 2nd ed. (Clarendon Press, Oxford, 1979).
- ²⁶ X.J.Chen,C.L.Zhang,J.S.Gardner,J.L.Sarrao, And C.C.Almasan, Phys.Rev.B68,064405(2003).
- ²⁷ B.I.Shklovskii and A.L.Efros, Electronic Properties of Doped Semiconductors (Springer-Verlag, Berlin, 1984).
- ²⁸ R.L.Zhang,W.H.Song, Y.Q.Ma,J.Yang,B.C.Zhao, Z.G.Sheng,J.M.Dai, and Y.P.Sun, Phys.Rev.B70,224418(2004).
- ²⁹ Sunil Nair and A.Banerjee, Phys.Rev.B70,104428(2004).
- ³⁰ S.Nakamae,D.Colson,A.Forget,I.Legros,J.F.Marucco, C.Ayache, and M.Ocio, Phys.Rev.B63,092407(2001).
- ³¹ I.P.Zvyagin, in Hopping Transport in Solids, edited by M. Pollak and B. Shklovskii (North-Holland, Amsterdam,1991)
- ³² M.Culter, and N.F.Mott, Phys.Rev.181,1336(1969).
- ³³ I.Maekawa,F.Takagi,Y.Sakai and N.Tsuda,J.Phys.Soc.Jpn.56,2119(1987).
- ³⁴ J.S.Zhou, J.B.Goodenough, and J.F.Mitchell,Phys.Rev.B58,R579(1998).
- ³⁵ M.Matsukawa,M.Narita,T. Nishimura,M.Yoshizawa, M.Apostu,R.Suryanarayanan, A.Revcolevschi,K.Itoh, and N.Kobayashi,, Phys.Rev.B67,104433(2003).